Constitutive Activation of Integrin α9 Augments Self-Directed Hyperplastic and Proinflammatory Properties of Fibroblast-like Synoviocytes of Rheumatoid Arthritis

Takashi Emori,*,† Jun Hirose,*,† Kotoko Ise,*,† Jun-ichiro Yomoda,*,† Michiko Kasahara,* Tadanobu Shinkuma,*,† Hiroyuki Yoshitomi,*,[1] Hiromu Ito,‡ Motomu Hashimoto,§ Shingo Sugahara,† Hirotada Fujita,† Nobuchika Yamamoto,† Yoshiaki Morita,*,† Shuh Narumiya,* and Ichiro Aramori*,†

Despite advances in the treatment of rheumatoid arthritis (RA), currently approved medications can have significant side effects due to their direct immunosuppressive activities. Additionally, current therapies do not address residual synovial inflammation. In this study, we evaluated the role of integrin α9 and its ligand, tenascin-C (Tn-C), on the proliferative and inflammatory response of fibroblast-like synoviocytes (FLSs) from RA patients grown in three-dimensional (3D)–micromass culture. FLSs from osteoarthritis patients, when grown in the 3D-culture system, formed self-directed lining-like structures, whereas FLSs from RA tissues (RA-FLSs) developed an abnormal structure of condensed cellular accumulation reflective of the pathogenic features of RA synovial tissues. Additionally, RA-FLSs grown in 3D culture showed autonomous production of proinflammatory mediators. Predominant expression of α9 and Tn-C was observed in the condensed lining, and knockdown of these molecules abrogated the abnormal lining-like structure formation and suppressed the spontaneous expression of matrix metalloproteinases, IL-6, TNFSF11/RANKL, and cadherin-11. Disruption of α9 also inhibited expression of Tn-C, suggesting existence of a positive feedback loop in which the engagement of α9 with Tn-C self-amplifies its own signaling and promotes progression of synovial hyperplasia. Depletion of α9 also suppressed the platelet-derived growth factor–induced hyperplastic response of RA-FLSs and blunted the TNF-α–induced expression of matrix metalloproteinases and IL-6. Finally, α9-blocking Ab also suppressed the formation of the condensed cellular lining by RA-FLSs in 3D cultures in a concentration-related manner. This study demonstrates the central role of α9 in pathogenic behaviors of RA-FLSs and highlights the potential of α9-blocking agents as a nonimmunosuppressive treatment for RA-associated synovitis. ***The Journal of Immunology*****, 2017, 199: 3427–3436.**

Rheumatoid arthritis (RA) is a pleiotropic autoimmune disease characterized by formation of hyperplastic synovial pannus tissue, which mediates joint destruction. Various agents, such as anti–TNF-α and anti–IL-6 receptor Abs, that are effective in suppressing active inflammation are currently available and have significantly advanced the treatment of RA. However, one shortcoming of these agents is that they raise the risk of infection by suppressing systemic immunity (1). Furthermore, examinations with advanced imaging techniques such as ultrasonography and magnetic resonance imaging have revealed persistent synovitis and tenosynovitis in more than a half of RA patients, even in patients in clinical remission with the above agents (2–4). Therefore, there remains an unmet medical need to prevent the joint damage by nonimmune mechanisms.

Fibroblast-like synoviocyte (FLSs) are the major component of synovial membrane and the predominant cell type of the aberrant pannus tissue. It has been suggested that inhibition of the hyperplastic response of FLSs in RA may present a complementary therapy without deleterious effect on immune responses (1). Under normal conditions, FLSs form a thin intimal layer lining of the synovium and protect joint by providing structural support and controlling the composition of the synovial fluid and extracellular matrix (ECM) (5). In the presence of the proinflammatory milieu that occurs in RA, FLSs undergo phenotypic conversion to FLSs from RA tissues (RA-FLSs), adopting various abnormal characteristics such as increased survival, adhesion, and invasiveness (1, 6). These RA-FLSs aggressively and autonomously condense to form a hyperplastic lining and, together with infiltrating inflammatory cells form an expansive synovial tissue, pannus. Cadherin-11, which is known to be responsible for cell–cell interactions between FLSs under physiological conditions also plays a crucial role in establishment of the hyperplastic cell condensation of RA-FLSs

*Center for Innovation in Immunoregulative Technology and Therapeutics, Graduate School of Medicine, Kyoto University, Kyoto 606-8501, Japan; †Drug Discovery Research, Astellas Pharma Inc., Ibaraki 305-8585, Japan; ‡Department of Orthopedic Surgery, Graduate School of Medicine, Kyoto University, Kyoto 606-8507, Japan; and §Department of the Control for Rheumatic Diseases, Graduate School of Medicine, Kyoto University, Kyoto 606-8507, Japan

[1]Current address: Department of Tissue Regeneration and Differentiation, Institute for Frontier Life and Medical Sciences, Kyoto University, Kyoto, Japan.

ORCIDs: 0000-0002-4908-1345 (H.F.); 0000-0003-4895-1596 (N.Y.); 0000-0001-8062-6529 (S.N.).

Received for publication June 29, 2017. Accepted for publication September 16, 2017.

This work was supported by the Special Coordination Funds for Promoting Science and Technology from Ministry of Education, Culture, Sports, Science and Technology and Astellas Pharma Inc.

Address correspondence and reprint requests to Dr. Ichiro Aramori, Drug Discovery Research, Astellas Pharma Inc., 21 Miyukiga-oka, Tsukuba, Ibaraki 305-8585, Japan. E-mail address: i.aramori@ak.med.kyoto-u.ac.jp

The online version of this article contains supplemental material.

Abbreviations used in this article: CAIA, collagen Ab–induced arthritis; 2D, two-dimensional; 3D, three-dimensional; ECM, extracellular matrix; FAK, focal adhesion kinase; FAKi, FAK inhibitor; FLS, fibroblast-like synoviocyte; KLH, keyhole limpet hemocyanin; OA, osteoarthritis; OA-FLS, FLS from OA tissue; PDGF, platelet-derived growth factor; RA, rheumatoid arthritis; RA-FLS, FLS from RA; shRNA, short hairpin RNA; Tn-C, tenascin-C.

(7–9). RA-FLSs not only produce their own proinflammatory mediators such as matrix metalloproteinase (MMP)-1, MMP-3, MMP-14, and TNFSF11 (also known as RANKL) (5, 10, 11), but they also respond to proinflammatory mediators in the inflammatory synovium, particularly to TNF-α, resulting in the production of proinflammatory mediators, including IL-6, platelet-derived growth factor (PDGF), TGF-β, and various MMPs, leading to establishment of chronic synovitis. Thus, RA-FLSs play a fundamental role in the pathogenesis of joint inflammation (1, 6, 9).

The cadherin-11–mediated cell–cell adhesion of FLSs and the integrin-mediated FLS adhesion to ECM have been reported to contribute to formation of the synovial lining and the hyperplasia in the synovial membrane (9, 12, 13), although the exact role of RA-FLS interaction with ECM in RA pathology remains to be fully elucidated. Integrins are composed of two subunits, α and β, and bind to ECM proteins such as fibronectin, laminins, collagens, and tenascins (14). Engagement of integrins with corresponding ECM ligand proteins activates intracellular signaling molecules, including focal adhesion kinase (FAK), Src, ERK, and PI3K, and regulates a wide range of cellular responses such as migration, survival, and proliferation (14). FAK is one of the first signaling molecules activated upon integrin engagement through autophosphorylation at Tyr^{397} and triggers outside-in integrin signaling (14). Src and PI3K act cooperatively with FAK in this pathway but also activate FAK-independent pathways (15, 16). Among various integrins expressed in FLSs, α9 is unique in that it does not bind to abundant ECM proteins such as fibronectin, laminins, vitronectin, or collagens but functions as a receptor for tenascin-C (Tn-C) (17), protease-cleaved osteopontin (18), VEGF-C (19), and thrombospondin-1 (20). Notably, expression of both α9 and Tn-C is augmented in synovial lining in RA (21), and pharmacological blockade of α9 has been shown to prevent synovial inflammation and joint destruction in the mouse model of arthritis (22). These findings suggest involvement of α9 in synovial inflammation. However, the role of α9 in the pathogenic behavior of RA-FLSs is poorly understood.

Previous studies have demonstrated that isolated RA-FLSs do not retain the intrinsic aggressiveness they show in primary tissues (23, 24). Recently, a unique three-dimensional (3D) culture system of RA-FLSs has been reported. In this system, isolated RA-FLSs not only establish hyperplastic lining-like aggressive cell assembly but also respond to TNF-α to produce proinflammatory cytokines, chemokines, and MMPs (25). The 3D-culture system thus appears to provide an in vitro model relevant to synovial hyperplasia in vivo and may be a powerful tool to analyze the abnormal behaviors intrinsic to RA-FLSs.

In the present study, using the 3D culture of patient-derived FLSs, we have shown that abnormally increased expression of α9 confers the abilities to RA-FLSs to form hyperplastic lining layers and enhances proinflammatory gene expression. Additionally, we provide evidence for involvement of α9 in the augmented response of RA-FLSs to TNF-α and PDGF. Our results have thus revealed the central role of α9 in the abnormal characteristics of RA-FLSs and highlight the therapeutic potential of α9 blockers to treat persistent synovitis in RA.

Materials and Methods

Inhibitor and blocking Abs

The FAK inhibitor (FAKi) PF-573228 was purchased from Sigma-Aldrich (St. Louis, MO). Etanercept (Enbrel) and natalizumab (Tysabri) were obtained from Pfizer (New York, NY) and Biogen (Cambridge, MA), respectively. Y9A2, a mouse IgG_1 Ab to human α9β1, was purified from the culture supernatants of hybridoma producing the Ab, provided by the University of California, San Francisco under a licensing agreement. ASP5094, a humanized Ab of Y9A2 with some beneficial mutations, was prepared as follows: DNA sequences encoding V region of H chain (V_H) and L chain (V_L) for improved blocking Ab to human α9 (26) were chemically synthesized and subcloned into pMK and pMA-T cloning vectors (Invitrogen, Waltham, MA), respectively, with attachment of HindIII (5′ end) and EcoRI (3′ end) sites. After confirmation of the entire sequences of the inserts, the DNA fragments were digested with HindIII and EcoRI, gel purified, and ligated into cassette expression vectors employing genes for C region of human IgG_1 (pEE6.4 for V_H and pEE12.4 for V_L, respectively) at the corresponding enzyme sites. Both vectors were licensed from Lonza Biologics (Basel, Switzerland). The resultant plasmids encoding complete amino acids for V_H and V_L of human IgG_1 were linearized by digestion with NotI and PvuI and ligated to each other to facilitate dual expression of both H and L chains from one plasmid according to the manufacturer's recommendation. Master cell bank was developed from Chinese hamster ovary cells stably transfected with the plasmid. ASP5094 was purified from the culture supernatants of the master cell bank and used in this study.

Patient-derived tissues

RA and osteoarthritis (OA) were diagnosed according to the criteria of the American College of Rheumatology (27, 28). Synovial tissues were obtained from OA and RA patients undergoing orthopedic surgery.

Isolation of FLSs

FLSs were isolated from synovial tissues as described previously (29). Briefly, the tissues were minced, digested, and cultured in DMEM (Life Technologies, Paisley, U.K.) supplemented with 10% heat-inactivated FBS (HyClone; GE Healthcare, Buckinghamshire, U.K.) and 100 U/ml penicillin and100 μg/ml streptomycin sulfate (Nacalai Tesque, Kyoto, Japan) in an incubator containing 5% CO_2 at 37°C. The adherent cells (which usually became observed after 7–14 d of culture) were cultivated to confluence. The cells were detouched from dishes by treatment with 0.05% trypsin solution containing 1 mM EDTA (Nacalai Tesque), split at a 1:3 ratio, and continuously cultured under identical conditions. The adherent cells, which had been passaged for 4–10 times after start of the culture, were used as isolated FLSs.

3D-micromass culture system

FLSs were resuspended in Matrigel (BD Biosciences, San Jose, CA) at a density of 4×10^6 cells/ml. Droplets of the cell suspension (35–45 μl) were placed onto 12-well culture plates coated with poly(2-hydroxyl methacrylate) (Sigma-Aldrich). After incubation at 37°C for 1 h to gelatinize the Matrigel, 1.5 ml of the culture medium was overlaid on the wells and the gelatinized droplets were floated by pipetting to start 3D-micromass culture. The floating cells in the Matrigel were maintained for 3 wk. Half of the culture medium was replaced twice a week throughout the culture period. In several experiments, the culture medium was supplemented with human TNF-α (20 ng/ml; R&D Systems, Minneapolis, MN) or human PDGF-BB (50 ng/ml; R&D Systems).

Immunofluorescent staining

Tissues or micromass architectures were embedded in Tissue-Tek OCT compound (Sakura Finetek, Tokyo, Japan), freeze-fixed, and sliced by cryostat. The thickness of the sections was set at 8 and 20 μm for tissues and micromass architectures, respectively. For immunofluorescence staining, the sections were fixed in PBS-buffered 4% paraformaldehyde for 10 min followed by permeabilization in ice-cold acetone for 5–10 min. The slides were blocked in PBS-buffered 1% BSA (Nacalai Tesque) and incubated with primary Abs overnight at 4°C, followed by incubation with fluorescent-labeled secondary Ab for 1 h. The primary and secondary Abs were diluted in PBS-buffered 1% BSA. In several experiments, DAPI (Dojindo, Kumamoto, Japan) was added to the diluent for secondary Ab at 1 μg/ml. For phalloidin staining, the slides were incubated with Alexa Fluor 488–labeled phalloidin (Life Technologies, Carlsbad, CA) diluted in PBS-buffered 1% BSA for 1 h. In several experiments, DAPI was added to the diluent. Acquisition of microscopic images was performed by an Axio Imager upright microscope with an HBO 100 microscope illuminating system (Carl Zeiss Microscopy, Oberkochen, Germany). Polyclonal Ab to human α9 was generated in rabbit by immunizing carrier protein–conjugated synthetic peptide corresponding to aa 674–685 (NRKENEDSWDWVQKNQ) in human α9 (NP_002198) and purified from the serum by protein A column. Other Abs used in this study listed below were purchased from the indicated venders: anti–Tn-C (mouse mAb; clone 3-C62, Wako Pure Chemical Industries, Tokyo, Japan) and anti-pFAK (pY397) (rabbit polyclonal Ab; ab39967, Abcam, Cambridge, U.K.).

Quantification of lining-like structure

Thickness of lining-like structure was measured by image analysis of phalloidin-stained sections of 3D-micromass architectures. Fluorescent microscopic images were obtained by NIS-Elements (version 3.2; Nikon, Tokyo, Japan). Area of the lining-like structure, stained by phalloidin, and perimeter of entire architecture section were measured by ImageJ software (version 1.47; National Institutes of Health, Bethesda MD). Average thickness of the lining-like structure was calculated as follows: thickness of lining-like structure = area of lining−like structure/perimeter of lining-like structure.

Blocking activity of ASP5094 on binding of α9-expressing cells to Tn-C–derived fragment

The blocking activity of ASP5094 on human α9 binding to the ligand was evaluated in previously reported adhesion assay of α9-expressing cells to Tn-C–derived peptide (21). Expression plasmid for human integrin α9 was constructed by inserting PCR-amplified *ITGA9* from human heart cDNA library into pcDNA3.1(−) mammalian expression vector (Invitrogen). To obtain cell clones stably expressing human α9, the plasmid was transfected to SW480 cells (American Type Culture Collection, Manassas, VA) with Lipofectamine (Invitrogen) and cultured in medium supplemented with Geneticin (1 mg/ml; Life Technologies) for a month. The enriched Geneticin-resistant cells were labeled with anti-α9 (Y9A2) in combination with FITC-labeled anti-mouse IgG (Life Technologies), and the cell population with high surface expression of α9 was isolated by FACS. A single-cell clone was further isolated from the population by standard cloning method and used for cell adhesion assay. Purified recombinant Tn-C peptide in which RGD sequence was mutated to RAA (Tn-Cfn3/RAA) was prepared as described elsewhere (17) and used as a ligand for α9-expressing cells. Blocking activity of ASP5094 on adhesion of α9-expressing cells to Tn-Cfn3/RAA was measured as follows: 96-well plates (MaxiSorp Immunoplate; Nalge Nunc, Rochester, NY) were coated with Tn-Cfn3/RAA (10 μg/ml) for 1 h at 37˚C. Wells similarly coated with PBS-buffered 1% BSA were also prepared to generate background value. After washing the plate with PBS, the wells were blocked with PBS supplemented with 0.5% BSA for 1 h, washed with PBS, and provided to adhesion assay. To determine the blocking activity of ASP5094, the α9-expressing SW480 cells (1×10^5) were resuspended in 200 μl of PBS containing 0.25% BSA with ASP5094 at the indicated concentrations (or with an equal volume of PBS for the control). The cells were transferred to the plate and incubated for 90 min in a CO_2 incubator to allow cell adhesion to the wells. After removal of nonadherent cells by washing with PBS twice, counts of the remaining cells were measured by CellTiter-Glo luminescent cell viability assay reagent (Promega, Madison, WI) according to the manufacturer's instructions. The value of each well was converted to percentage of control after subtraction of the background value generated by binding of PBS-treated cells to the BSA-coated wells. The IC_{50} value was calculated by GraphPad Prism 5 software (version 5.04; GraphPad Software, La Jolla, CA) with nonlinear regression curve fitting. The final IC_{50} value was determined as the geometric mean of three independent calculations.

Real-time PCR

Total RNA was extracted by Isogen (Nippon Gene, Tokyo, Japan) and further purified by an RNeasy Plus micro kit (Qiagen, Hilden, Germany) (for 3D-cultured cells and tissues) or directly purified by an RNeasy Plus micro kit (for plate-cultured cells) according to the manufacturers' instructions. cDNA was synthesized by the RT-PCR system for first-strand cDNA synthesis (Thermo Fisher Scientific) using 100–500 ng total RNA. Real-time PCR was performed using Thunderbird probe quantitative PCR mix (Toyobo, Osaka, Japan) with gene-specific TaqMan probes in a ViiA7 real-time PCR system (Applied Biosystems, Foster City, CA). PCR reaction was performed as follows: denaturation at 94˚C for 1 min followed by 45 cycles at 95˚C for 15 s, 55˚C for 45 s. Expression levels of each gene were normalized by those of *GAPDH* in in vitro experiments. Expression levels of *Hprt* were used for the normalization in the analysis of animal study (30). The following gene-specific TaqMan probes were purchased from Applied Biosystems and used in this work: probes for human genes: *ITGA1* (Hs00235006_m1), *ITGA2* (Hs00158127_m1), *ITGA4* (Hs00168433_m1), *ITGA5* (Rn01761831_m1), *ITGA6* (Hs01041011_m1), *ITGA9* (Hs00979865_m1), *ITGAV* (Hs00233808_m1), *ITGB1* (Hs00559595_m1), *TNC* (Hs01115665_m1), *LAMA1* (Hs00300550_m1), *COL1A1* (Hs00164004_m1), *FN1* (Hs01549976_m1), *MMP1* (Hs00899658_m1), *MMP3* (Hs00968305_m1), *MMP14* (Hs01037003_g1), *IL6* (Hs00985639_m1), *TNFSF11* (Hs00243522_m1), *GAPDH* (Hs02758991_g1), *CDH11* (Hs00901475_m1). Probes for mouse genes; *Itga9* (Mm00519317_m1), *Tnc* (Mm00495662_m1), *Cdh11* (Mm00515466_m1), *Mmp1a* (Mm00473485_m1), *Mmp1b* (Mm00473493_m1), *Mmp3* (Mm00440295_m1), *Il6* (Mm00446190_m1), *Hprt* (Mm03024075_m1).

Western blotting

Cells cultured in either a 3D-micromass system or tissue culture plate were lysed in TNEU buffer (50 mM Tris-HCl, 150 mM NaCl, 1 mM EDTA, 4 M urea, 1% SDS [pH 7.8]) and clarified by centrifugation. Protein concentration of the lysates was determined by a micro BCA protein assay kit (Pierce, Rockford, IL) using BSA as a standard. Ten to fifty micrograms of the lysates was separated in SDS-PAGE and transferred to polyvinylidene difluoride membranes. The membranes were blocked with Blocking One (Nacalai Tesque) and incubated with primary Ab overnight at 4˚C, followed by incubation with HRP-conjugated secondary Ab for 1 h. The primary and secondary Abs were diluted in Can Get Signal immunoreaction enhancer solution (Toyobo). The membranes were developed with Super-Signal West Dura extended duration substrate (Pierce) and imaged on an LAS-4000 mini luminescent image analyzer system (Fuji Film, Tokyo, Japan). The Abs used in the experiments were as follows: anti-human α9 (rabbit mAb; ab140599; Abcam), anti-human Cadherin-11 (rabbit polyclonal Ab; LS-B2308; LSBio, Seattle, WA), anti–Tn-C (mouse mAb; clone 4F10TT; Immuno-Biological Laboratories, Gunma, Japan), anti–total FAK (rabbit mAb; 3285; Cell Signaling Technology, Danvers, MA), anti-pFAK (pY397) (rabbit mAb; 8556; Cell Signaling Technology), anti–MMP-14 (goat pAb, AF918; R&D Systems), anti-TNFSF11 (goat pAb; AB626; R&D Systems), HRP-conjugated anti-mouse IgG (NA931V; GE Healthcare), and HRP-conjugated anti-rabbit IgG (NA934V; GE Healthcare).

Knockdown experiments with lentivirus-introduced short hairpin RNA

Lentivirus short hairpin RNA (shRNA) expression plasmids for *ITGA9* (TRCN0000230788), *TNC* (TRCN0000057740), control shRNA plasmid (pLKO.1-puro non-mammalian shRNA control plasmid DNA), and lentiviral packaging mix were purchased from Sigma-Aldrich. The recombinant lentivirus was produced by 293T cells (Takara Bio, Shiga, Japan) in 100-mm dishes according to instructions attached to the packaging mix. Briefly, 4×10^6 293T cells were seeded in type I collagen–coated 100-mm dishes (AGC Techno Glass, Shizuoka, Japan), followed by transfection with expression plasmid (2.6 μg) mixed with packaging mix (26 μg) using FuGENE6 transfection reagent (Promega) on the next day. After 16 h of transfection, the culture supernatants were completely removed and replaced to fresh media, followed by incubation for 48 h to allow production of recombinant lentivirus in the supernatants. After removal of debris by centrifugation, the supernatants were concentrated by Lenti-X concentrator (Takara Bio) for 10-fold and used in infection experiments. For infection of the lentivirus to RA-FLSs, the cells were seeded at 2×10^5 in six-well plates. On the following day, the culture media were completely removed and 1 ml of lentivirus aliquots containing 12 μg/ml hexadimethrine bromide (also termed Polybrene, Sigma-Aldrich) was added to the wells. After incubation at 20˚C for 2 h, 2 ml of fresh medium was added to each well. After following incubation at 37˚C for 72 h, the cells were detouched, counted, and provided to further experiments.

ELISA

Amounts of secreted proteins in the culture supernatants were determined by ELISA assays using commercially available kits as follows: MMP-1 (human gotal MMP-1 DuoSet ELISA; R&D Systems), MMP-3 (human total MMP-3 DuoSet ELISA; R&D Systems), IL-6 (human IL-6 DuoSet ELISA; R&D Systems), Tn-C (Tn-C large [FNIII-B] ELISA; Immuno-Biological Laboratories).

Mouse collagen Ab-induced arthritis model

Mouse IgG_1 mAb for keyhole limpet hemocyanin (KLH) was obtained from hybridoma expressing anti-KLH IgG_1 in our laboratory and used as a control. MA9-413, a mouse α9-blocking single-chain variable fragment of Ig fused to mouse IgG_1, was prepared as described above. Male DBA/1J mice (7 wk of age) were purchased from Charles River (Yokohama, Japan) and housed in a specific pathogen-free environment in an animal facility of Kyoto University. Mice were divided into three groups ($n = 8$ per group) on day −1, and arthritis was induced by injection of anti-collagen Ab mixture (1.5 mg per mouse; Chondrex, Redmond, WA) on day 0, followed by injection of LPS (50 μg per mouse; Chondrex) on day 3. Control mouse IgG_1 (30 mg/kg) and M9-413 (10 and 30 mg/kg) were administered on days 0, 2, 4, 6, 8, 10, and 12 and the study was ended on day 13. Injection of anti-collagen Ab, LPS, control IgG_1, and MA9-413 was performed via i.p. administration. Joint swelling was scored on days 0, 3, 5, 7, 10, and 13 as described elsewhere (31). On day 13, paws were fixed in 10% neutral

formalin (Nacalai Tesque), decalcified in EDTA-based neutral decalcifying solution (Wako pure chemical), and provided to histological analysis (left hindlimbs). The right hindlimbs were provided to real-time PCR after removal of skins.

Pathological analyses and immunohistochemistry

Paraffin-embedded joint tissues from collagen Ab–induced arthritis (CAIA) mice were sliced at 3-μm thickness and stained with H&E for pathological analysis. The severity of synovial hyperplasia and bone resorption was scored by five-grade evaluation (0–4) according to the previously reported criteria (32) with slight modifications as follows: for hyperplasia: 0, normal; 1, minimal infiltration of pannus in cartilage and subchondral bone of marginal zone; 2, mild infiltration of marginal zone with minor cortical and medullary bone destruction; 3, moderate infiltration with moderate hard tissue destruction; 4, severe infiltration associated with total or near total destruction of joint architecture; for bone resorption: 0, normal; 1, small areas of marginal zone/periosteal resorption, not readily apparent on low magnification; 2, more numerous areas of marginal zone/periosteal resorption, readily apparent on low magnification, minor overall cortical and medullary bone loss; 3, obvious resorption of medullary trabecular and cortical bone without full thickness defects in entire cortex, loss of some medullary trabeculae, lesion apparent on low magnification; 4, full thickness defects in cortical bone and destruction of joint architecture.

Immunohistostaining was performed according to standard procedures. Briefly, the sections were incubated in 0.3% H_2O_2 for 20 min, blocked with PBS-buffered 1% BSA for 1 h, and incubated overnight at 4°C with rabbit anti-pFAK (pY397) Ab (10 μg/ml; ab39967; Abcam). The sections were then incubated with HRP-conjugated anti-rabbit IgG for 1 h at room temperature and visualized with diaminobenzidine.

Study approval

Ethical approval for this study was granted by the Ethics Committee of Kyoto University Graduate School and Faculty of Medicine and Astellas Research Ethics Committee. Informed consent was obtained from all the patients prior to sample collection. Animal studies were approved by the Institutional Animal Care and Use Committee of Kyoto University Graduate School of Medicine.

Statistical analysis

Statistical analyses were performed by GraphPad Prism 5 software (version 5.04; GraphPad software, Figs. 1, 2, 3A, 4A, 4C, 5) and SAS software (SAS Institute, Figs. 3D, 4B, 6, 7C, 7D, Supplemental Figs. 1, 2). A p value <0.05 was considered statistically significant.

Results

The 3D-micromass culture system reproduces disease-related aggressive behavior of RA-FLSs

To examine whether the ability to condense into the lining is intrinsic and specific to RA-FLSs or shared by FLSs in other arthritic diseases, RA-FLSs and FLSs from OA tissues (OA-FLSs) were isolated and cultured in a 3D-micromass system. The resultant cell architectures on micromass were freeze-fixed, sectioned, and stained with DAPI. Both RA- and OA-FLSs assembled at the interface between the matrix and the fluid phase in 3D-culture, but their architectures were markedly different. The lining-like architecture formed by RA-FLSs frequently showed regions of condensed cellular accumulation several cells deep, which was reminiscent of the synovial lining architecture in RA patients (Fig. 1A, right). In contrast, OA-FLSs formed mostly single-cell layered lining, and areas of condensed cellular accumulation were rarely seen (Fig. 1A, left). To analyze the lining-like structure, sections were stained with fluorescent-labeled phalloidin. Consistent with a previous report (7), the condensed cells displayed actin fibers, and the lining-like architecture was intensely visualized as a whole (Fig. 1B). Measurement of the phalloidin-stained areas revealed that the lining architecture by RA-FLSs was significantly thicker than that by OA-FLSs (Fig. 1C). These results indicate that RA-FLSs have the intrinsic ability to form condensed synovial architecture that may drive the formation of hyperplastic synovial linings in vivo.

Given that the 3D-culture system of FLSs reproduced the structural features of synovial tissues, we next examined whether the 3D culture of FLSs could restore their ability to produce proinflammatory mediators in vitro. To address this question, real-time PCR was used to determine the expression levels of *MMP1*, *MMP3*, *MMP14*, *IL6*, and *TNFSF11* (genes encoding MMP-1, MMP-3, MMP-14, IL-6, and TNFSF11, respectively) in FLSs. The expression of these proinflammatory genes in the 3D culture of RA- and OA-FLSs was markedly enhanced compared with that observed in the same cell types grown in two-dimensional (2D) culture (Fig. 1D). Additionally, the expression levels of *MMP1*, *MMP3*, and *TNFSF11* in 3D culture were significantly higher in RA-FLSs than in OA-FLSs (Fig. 1D). Although not reaching a level of statistical significance, the expression levels of *IL6* also tended to be higher in RA-FLSs (Fig. 1D). These findings indicate that RA-FLSs grown in 3D culture retain elevated proinflammatory gene expression seen in primary synovial tissues. Thus, the 3D-culture system recapitulates the self-directed aggressive behavior of RA-FLSs displayed in the synovial lining in vivo.

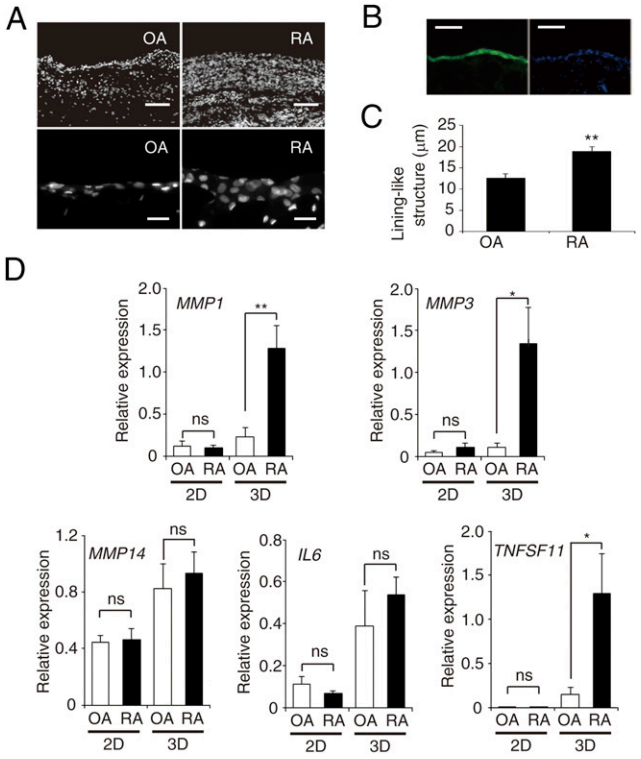

FIGURE 1. Aggressive behavior of RA-FLSs reproduced in the 3D-micromass system. (**A**) Typical microscopic images of arthritic synovial lining layer and in vitro established lining-like structure. Frozen sections of synovial tissues from OA and RA (upper), or 3D-cultured micromass architecture formed by OA- and RA-FLSs (lower), were stained with DAPI. Scale bars, 100 μm. (**B**) Section from 3D-culturted micromass architecture formed by RA-FLSs costained with Alexa Fluor 488–phalloidin (left) and DAPI (right). Scale bars, 200 μm. (**C**) Comparison of thickness of lining-like structure established by OA- and RA-FLSs. Frozen sections of micromass architectures formed by OA- ($n = 5$) and RA-FLSs ($n = 5$) were stained by Alexa Fluor 488–phalloidin. Thickness of the structure was calculated by image analysis and expressed as mean ± SE. (**D**) Analysis of proinflammatory gene expression in OA- ($n = 5$) and RA-FLSs ($n = 5$) cultured in either monolayer (2D) or 3D-culture system (3D). Relative expression level of indicated genes was determined by real-time PCR and expressed as mean ± SE. Statistical analyses were performed by a Student t test (C and D). $^*p < 0.05$, $^{**}p < 0.01$. ns, not significant.

Activation of FAK-mediated signaling causes the aggressive behavior of RA-FLSs in 3D culture

To address the signaling mechanism responsible for the above pathological behavior of RA-FLSs in 3D culture, we first examined the phosphorylation level of FAK in RA tissues and compared it with that in OA tissues. Frozen sections from the synovial tissues from RA and OA stained with Ab to pFAK were examined by fluorescence microscopy. Phosphorylation of FAK was marked in the lining of RA synovium, whereas pFAK was minimally seen in OA tissues (Fig. 2A). Phosphorylation of FAK in RA-FLSs in 2D or 3D culture was then assessed by Western blotting. RA-FLSs cultured under 3D but not under 2D conditions showed phosphorylation of FAK (Fig. 2B), indicating that the increased FAK-mediated signaling seen in synovial lining cells in vivo were maintained in the 3D-culture system.

Because these results indicated that RA-FLSs have an activated FAK pathway relative to OA-FLSs, we next examined the contribution of FAK activation to the proinflammatory character of RA-FLSs. RA-FLSs maintained in 3D culture in the presence of a FAKi (10 μM PF-573228) showed marked decreases in proinflammatory mediator gene expression compared with RA-FLSs cultured in the absence of PF-573228 (86.9, 98.3, and 55.4% inhibition of the control for *MMP1*, *MMP3*, and *IL6*, respectively) (Fig. 2C). Because FAK phosphorylation is induced by integrin activation, these results indicate that FAK-mediated integrin signaling plays a crucial role in the intrinsic production of proinflammatory mediators by RA-FLSs.

Depletion of α9 or Tn-C suppresses hyperplastic and proinflammatory phenotype of RA-FLSs in 3D culture

To identify molecules that trigger constitutive activation of the integrin signaling in 3D-cultured RA-FLSs, we examined expression of genes for various integrins and their ligands in 3D-cultured RA- and OA-FLSs. Notably, the expression of *ITGA9* and *TNC* (encoding α9 and Tn-C, respectively) were significantly higher in RA-FLSs than in OA-FLSs (Fig. 3A, left, middle), whereas no significant differences were observed in expression of *ITGA1*, *2*, *4*, *5*, *6*, *V*, and *ITGB1* (encoding integrin α1, α2, α4, α5, α6, αV, and β1, respectively, Supplemental Fig. 1A), Additionally, the expression of *LAMA1* and *FN1* (encoding laminin A1 and fibronectin, respectively) by RA- and OA-FLSs were not significantly different (Supplemental Fig. 1B). Furthermore, immunofluorescence staining revealed colocalization of α9 and Tn-C proteins in the lining-like structure formed by 3D culture of RA-FLSs (Fig. 3A, right). The clinical relevance of this finding was validated in primary synovial tissues from RA patients where deposition of Tn-C was observed around α9-positive cells (Fig. 3A, right). These results suggest that α9 is significantly upregulated in 3D-cultured RA-FLSs and that it binds to its ligand, Tn-C, which is produced by RA-FLSs themselves and also upregulated in 3D culture. These results suggest that interaction of α9 on RA-FLSs with Tn-C activates the integrin signaling pathway in the synovial lining.

To examine the role of α9 and Tn-C in hyperplastic and proinflammatory phenotype in 3D culture, RA-FLSs were transfected with shRNA for *ITGA9*, *TNC*, or control scrambled shRNA by lentivirus vector and subjected to 3D-micromass culture. Western blotting of the cell lysates and ELISA of the culture supernatants confirmed successful knockdown of *ITGA9* and *TNC* in the experimental period (Supplemental Fig. 2). Despite depletion of α9 and Tn-C, RA-FLSs moved to the interface between the matrix and the fluid phase. However, the appearance of cell assembly analyzed by phalloidin staining was dramatically altered. Whereas the cells treated with the control shRNA formed condensed structural assembly with densely packed actin bundles (Fig. 3B), the cells treated with the shRNA either for *ITGA9* or *TNC* displayed loose cell aggregates with much less phalloidin staining (Fig. 3C). These observations indicate that depletion of either α9 or Tn-C disrupted the ability of RA-FLSs to form condensed cell assembly.

We next examined the effect of α9 and Tn-C depletion on activation of FAK-mediated integrin signaling. Knockdown of either

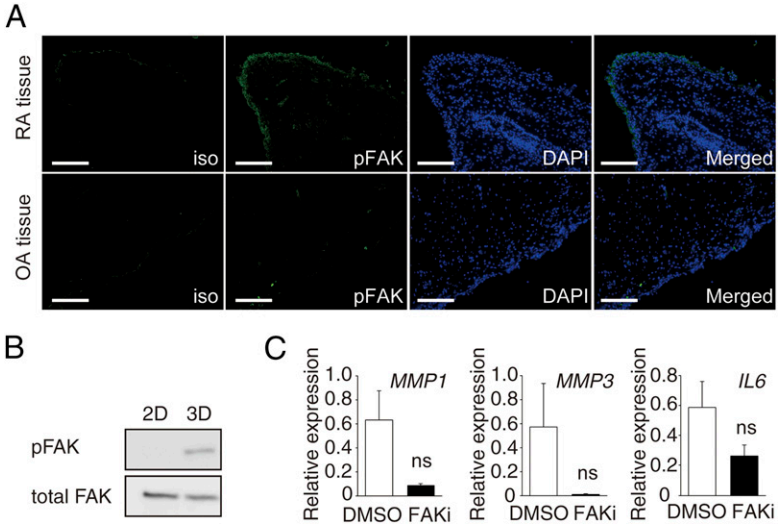

FIGURE 2. Involvement of FAK activation in the autonomous expression of proinflammatory genes in 3D-cultured RA-FLSs. (**A**) Fluorescent microscopic analyses of FAK phosphorylation status in RA and OA synovial tissues. Frozen sections from RA (upper) and OA synovial tissues (lower) were stained with isotype-matched control Ab (iso), anti-phosphorylated FAK Ab with Alexa Fluor 488–labeled secondary Ab (pFAK), and DAPI. The slides were photographed under fluorescent microscopy with the same exposure time. Representative images from three independent patients' tissues are shown. Scale bars, 200 μm. (**B**) Western blot analysis of phosphorylated status of FAK in 3D-cultured RA-FLSs. Cell lysates prepared from plate-cultured (2D) or 3D-cultured (3D) RA-FLSs were analyzed in Western blotting with anti-pFAK (upper) or anti-total FAK (lower) Abs. (**C**) Real-time PCR analysis of proinflammatory gene expression in 3D-cultured RA-FLSs treated with FAKi (10 μM PF-573228, $n = 5$) or the control (0.01% DMSO, $n = 5$). The data were expressed as mean ± SE. Statistical analyses were performed by a paired t test. ns, not significant.

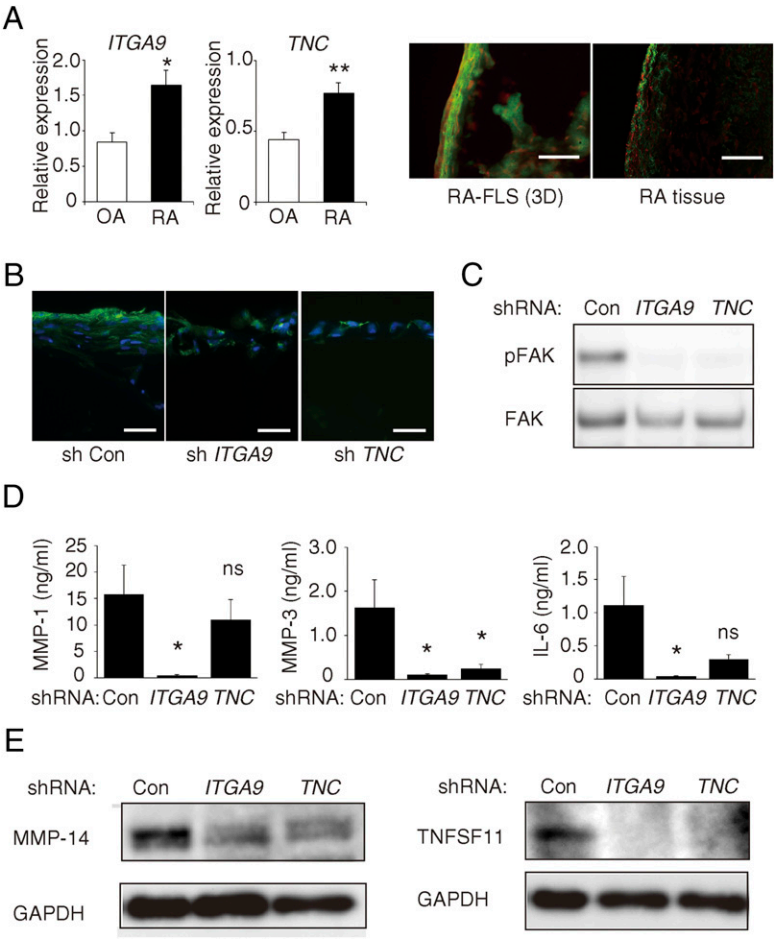

FIGURE 3. Involvement of α9 and Tn-C in the self-directed abnormal behavior of RA-FLSs. (**A**) Gene expression levels of *ITGA9* (left) and *TNC* (middle) in OA- ($n = 5$) and RA-FLSs ($n = 5$) were determined by real-time PCR and expressed as mean ± SE. Distributions of α9 and Tn-C in 3D-cultured RA-FLSs and RA synovial tissue was determined by costaining with Alexa Fluor 594–labeled Ab to α9 (red) and Ab to Tn-C with Alexa Fluor 488–labeled secondary Ab (green) (right). Scale bars, 100 μm. (**B**–**E**) RA-FLSs treated with shRNA either for *ITGA9*, *TNC*, or the control (Con) cultured in 3D micromass were analyzed the phenotypes. (B) Sections from the resultant architectures were costained with Alexa Fluor 488–phalloidin (green) and DAPI (blue). Representative data from three independent RA-FLSs are shown. Scale bars, 50 μm. (C) Cell lysates from 3D-cultured RA-FLSs were analyzed by Western blotting with Abs to pFAK (upper) and total FAK (lower). Representative data from five independent blots are shown. (D) Protein amounts of MMP-1, MMP-3, and IL-6 in the culture supernatants were determined by ELISA and indicated as mean ± SE ($n = 5$). (E) Western blotting of the cell lysates with Abs to MMP-14 (left), TNFSF11 (right) and GAPDH. A representative data from five independent blots was shown. Statistical analyses were performed by a Student t test (A) and a Dunnett test using within-subject error (D). $^*p < 0.05$, $^{**}p < 0.01$. ns, not significant.

ITGA9 or *TNC* in RA-FLSs in 3D culture blocked phosphorylation of FAK (Fig. 3C). Furthermore, similar to the findings of the FAKi-treated RA-FLSs in 3D culture, knockdown of either *ITGA9* or *TNC* in RA-FLSs markedly decreased the amount of MMP-1, MMP-3, and IL-6 present in the culture supernatants (Fig. 3D). Protein expression of MMP-14 and TNFSF11 was also suppressed by knockdown of either *ITGA9* or *TNC* (Fig. 3E). The suppression of MMP-1, MMP-3, and IL-6 production was more prominent in *ITGA9*-deficient cells than in *TNC*-deficient cells. Several α9 ligands produced by RA-FLSs, such as thrombospondin-1 (33) and VEGF-C (34), might complement the lack of Tn-C by treatment with shRNA at least in part. These results indicate that depletion of α9 and Tn-C induces the same phenotypes as that seen by blocking FAK activation, and they suggest that Tn-C acts as a ligand of α9 in 3D-cultured RA-FLSs and this α9/Tn-C axis triggers FAK-mediated integrin signaling that is involved in the self-directed cellular assembly and proinflammatory mediator release for development of RA pathology.

In addition to the above alterations of intrinsic proinflammatory properties, we found that depletion of α9 resulted in decreased gene and protein expression of Tn-C in 3D-cultured RA-FLSs (Fig. 4A). Similarly, we found suppressed *TNC* expression by disruption of FAK signaling by treatment with FAKi (Fig. 4C, left). These observations indicate that production of Tn-C is dependent on α9-dependent FAK activation in integrin signaling, suggesting that engagement of α9 with Tn-C leads to further expression of Tn-C and continuous activation of α9. Such a self-amplifying positive feedback loop accelerates pathogenic behavior of RA-FLSs and promotes sustained inflammation.

As described above, depletion of either α9 or Tn-C by shRNA almost completely abolished the formation of actin bundles in 3D-cultured RA-FLSs. These observations led us to examine expression of cadherin-11, which is responsible for cell–cell adhesion between FLSs and stimulates actin remodeling in RA-FLSs (7). Strikingly, RA-FLSs treated with either of the shRNAs significantly decreased the expression of cadherin-11 in both mRNA and protein levels (Fig. 4B), indicating that α9/Tn-C signaling is involved in the expression of cadherin-11. The expression of *CDH11* (encoding cadherin-11) was not inhibited by treatment with FAKi in 3D-cultured RA-FLSs (Fig. 4C, right), suggesting the possible involvement of FAK-independent pathways in regulation of cadherin-11 expression beyond α9 engagement. FAK-independent PI3K signaling triggered by α9 activation (15, 16) might play an important role in increasing cadherin-11 expression in FLSs under inflammatory conditions (35).

Role of α9 is indispensable for RA-FLS responses to inflammatory stimuli

Although α9 plays a key role in the autonomous aggressive behavior of RA-FLSs, it remains uncertain whether it also contributes to exogenous inflammatory stimuli, often called the "passive" inflammatory responses of RA-FLSs. Hence, the roles of α9 in responses of RA-FLSs to exogenously applied stimuli (PDGF and TNF-α) were determined in 3D culture. RA-FLSs transfected with shRNA for *ITGA9* or scrambled control shRNA were grown in 3D culture with medium supplemented with PDGF or TNF-α. Incubation of the control shRNA-transfected RA-FLSs with PDGF resulted in thickening of the cellular structure as determined by phalloidin staining (Fig. 5A, upper). Control shRNA-transfected

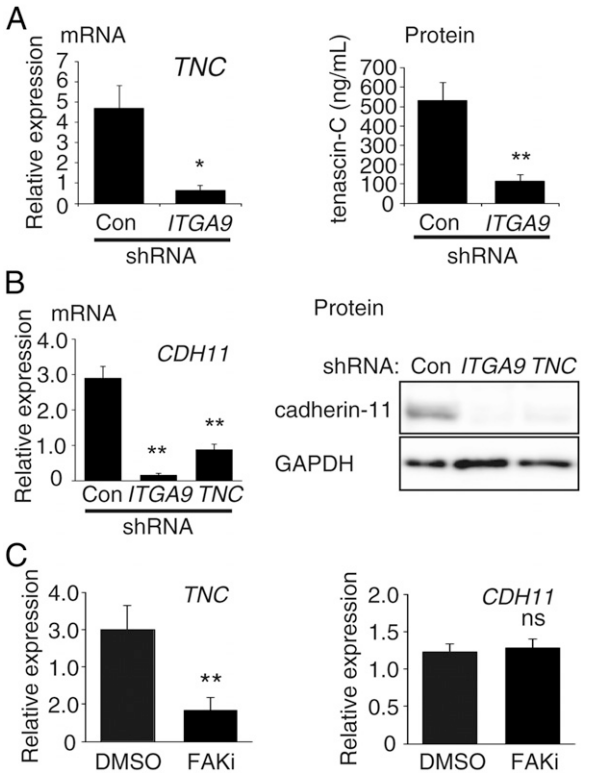

FIGURE 4. Expression levels of Tn-C and cadherin-11 in 3D-cultured RA-FLS treated with shRNA for *ITGA9*, *TNC*, or FAKi. (**A**) Gene and protein expression levels of Tn-C in 3D-cultured RA-FLSs treated with shRNA for *ITGA9* were determined by real-time PCR ($n = 5$, left) and ELISA with the culture supernatants ($n = 5$, right), respectively. (**B**) Gene and protein expression levels of cadherin-11 in 3D-cultured RA-FLSs treated with the indicated shRNA were determined by real-time PCR ($n = 5$, left) and Western blotting with Abs to cadherin-11 and GAPDH (right), respectively. Representative data from five independent blots are shown. (**C**) Gene expression levels of *TNC* (left) and *CDH11* (right) in 3D-cultured RA-FLSs treated with or without FAKi were determined by real-time PCR with total RNA prepared in Fig. 2C ($n = 5$) and expressed as mean ± SE ($n = 5$). Statistical analyses were performed by a paired *t* test (A and C) and a Dunnett test using within-subject error (B). $^{*}p < 0.05$, $^{**}p < 0.01$. ns, not significant.

RA-FLSs incubated in 3D culture with TNF-α did not show this response (Fig. 5A, upper). These findings were consistent with reports in the literature (25, 29) and validated the assay response. Conversely, RA-FLSs transfected with shRNA for *ITGA9* did not condense into lining-like architecture nor did it exhibit a hyperplastic response to PDGF (Fig. 5A, lower).

Alternatively, RA-FLSs transfected with control shRNA and grown in 3D cultures with TNF-α showed significantly enhanced production of MMP-1, MMP-3, and IL-6. The release of these proinflammatory mediators in response to exogenous TNF-α was almost completely absent in 3D culture of RA-FLSs transfected with shRNA for *ITGA9* (Fig. 5B, 99.4, 97.2, and 91.0% inhibition of the control, respectively). These results indicate that α9-mediated signaling in 3D-cultured RA-FLSs is required not only for the hyperplastic response to PDGF but also for the production of proinflammatory mediators in response to TNF-α. These data indicate that α9 plays a pivotal role in the passive inflammatory responses of 3D-cultured RA-FLSs to exogenous inflammatory mediators.

Pharmacological blockade of α9 signaling suppresses development of synovitis in mouse arthritis model

The above results show that α9 signaling mediates the expression of Tn-C, cadherin-11, MMPs, and IL-6 and elicits the two pathogenic features in 3D-cultured RA-FLSs, intrinsic hyperplastic and aggressive behavior and passive inflammatory responses. We therefore addressed whether such α9-mediated mechanisms could also play a role in synovial hyperplasia observed in a mouse arthritis model. A mouse α9-blocking single-chain variable fragment of Ig fused to mouse IgG_1, termed MA9-413 (36), was generated and used in this experiment. The isotype control for this study was mouse IgG_1 mAb to KLH. The CAIA model was chosen to test the effects of MA9-413 because it results in the development of severe arthritis with synovial lining hyperplasia

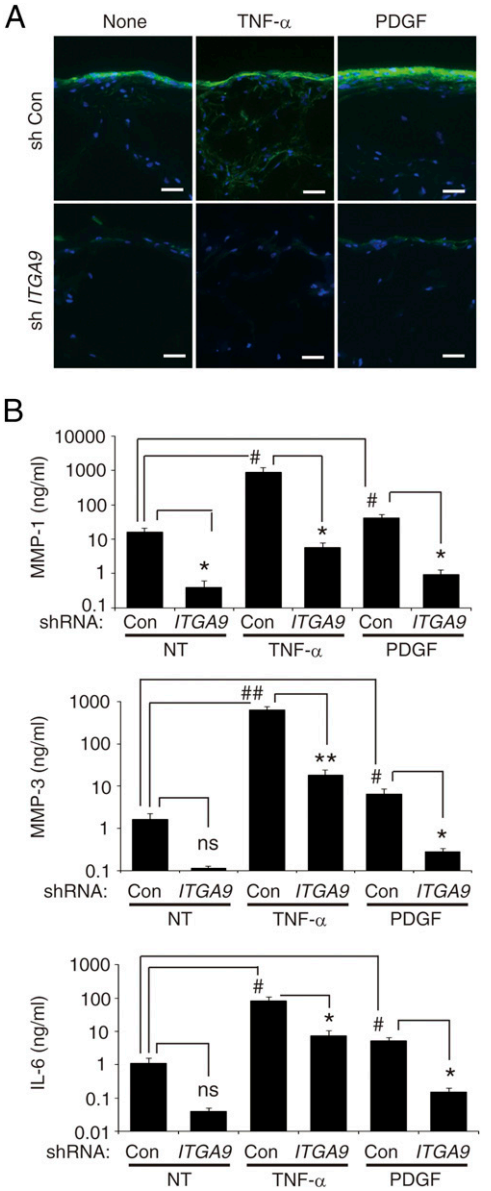

FIGURE 5. Phenotypes of RA-FLSs with depletion of α9 cultured in 3D-micromass system under stimulation with PDGF or TNF-α. RA-FLSs treated with shRNA either for *ITGA9* or the control (Con) were cultured in a 3D-micromass system in the media supplemented with PDGF (PDGF-BB, 50 ng/ml) or TNF-α (20 ng/ml) and the phenotypes were analyzed. (**A**) Frozen sections from the resultant architectures were costained with Alexa Fluor 488–phalloidin (green) and DAPI (blue). Representative data from three independent experiments are shown. Scale bars, 50 μm. (**B**) Protein amounts of MMP-1, MMP-3, and IL-6 in the culture supernatants collected at the end of the study were determined by ELISA and expressed as mean ± SE ($n = 5$). Statistical analyses were performed by a paired *t* test. $^{*/\#}p < 0.05$, $^{**/\#\#}p < 0.01$. ns, not significant.

(37). Administration of MA9-413, but not the control IgG_1, suppressed the development of ankle joint swelling in a dose-related manner (Fig. 6A), and it significantly suppressed hyperplasia and bone resorption (Fig. 6B). These results indicate that α9 plays an important role in the development of synovial lining hyperplasia leading to bone resorption in the CAIA joints. Furthermore, gene expression analysis revealed that, although expression of both *Itga9* and *Tnc* (genes encoding mouse α9 and Tn-C) in the arthritic ankle of mice administered the control IgG_1 were markedly elevated (Fig. 6C), the expression of these genes was significantly attenuated in mice treated with MA9-413 (Fig. 6C). This is in good agreement with the data in 3D-cultured RA-FLSs (Fig. 3A).

We further analyzed the state of integrin signaling in the joints by immunohistochemical staining. Similar to the results in RA tissues and 3D-cultured RA-FLSs (Fig. 2A, 2B), signals for pFAK were intensively localized in the hyperplastic lining of the arthritic joints of the mice administrated the control IgG_1. Mice treated with MA9-413 showed diminished phosphorylation of FAK in the arthritic joint to levels similar to that seen in nonarthritic joints (Fig. 6D). These results indicate that α9 activates the FAK signaling pathway in the hyperplastic synovial lining from CAIA joints.

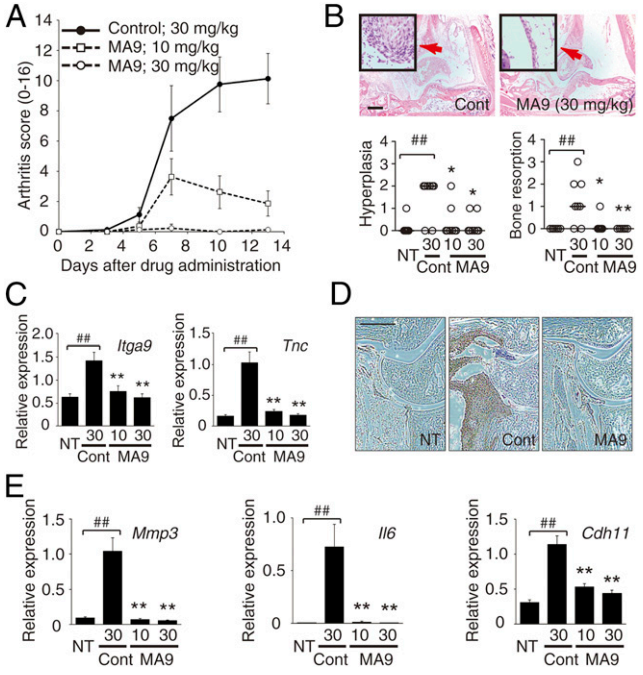

FIGURE 6. Effects of pharmacological blockade of α9 in development of synovial hyperplasia in CAIA model. (**A**) Changes in the arthritis scores of each group. Data indicate mean ± SE. ●, control; □, MA9-413 (10 mg/kg); ○, MA9-413 (30 mg/kg). (**B**) Pathological analysis of the inflamed joints. Sections from the left hindlimbs were stained with H&E. The black boxes indicate the close-up images of synovial lining (red arrows). Scale bars, 500 μm (upper). Severity of synovial hyperplasia and bone resorption was scored (0–4) and expressed as dotted plot. ○, individual scores; bars, median. Statistical analyses were performed by Wilcoxon rank sum test (NT; normal versus control groups) and a Steel multiple comparison test (control versus MA9-413-treated groups). $*p < 0.05$, $^{\#\#}{*}*p < 0.01$. (**C** and **E**) Gene expression analysis of the inflamed joints. Total RNA from right hindlimbs of NT, control, and MA9-413–treated groups was analyzed by real-time PCR. The data indicate mean ± SE. Statistical analyses were performed by a Student *t* test (NT versus control groups) and a Dunnett test (control versus MA9-413–treated groups). $^{\#\#}{*}*p < 0.01$. ns, not significant. (**D**) Immunohistostaining of the CAIA joints. Sections from the left hindlimbs were stained with Ab to pFAK. Representative data from the indicated groups are shown. Scale bars, 500 μm.

To examine the effect of MA9-413 on α9-mediated gene expression in the joints further, *Mmp1*, *Mmp3*, *Il6*, and *Cdh11* expression levels (genes encoding mouse MMP-1, MMP-3, IL-6, and cadherin-11, respectively) were determined by real-time PCR. The expression of *Mmp3*, *Il6*, and *Cdh11* was upregulated in the arthritic joint from mice treated with the control IgG_1 (Fig. 6E) although the expression of *Mmp1* was not detected. Administration of MA9-413 significantly suppressed expression levels of these genes (Fig. 6E), which is in accordance with the results of depleting α9 in vitro (Figs. 3D, 4A, 4B). These results indicate that α9 mediates enhanced expression of MMP-3, IL-6, and cadherin-11 in the CAIA joints.

Taken together, the data suggest that activation of α9 plays an important role in the development of synovial lining hyperplasia and production of inflammatory mediators in vivo.

Humanized anti-α9 Ab, ASP5094, suppresses self-directed hyperplastic behavior of RA-FLSs

The above results taken together suggest that α9 overexpressed in RA tissue may function as a driver of chronic synovitis in vivo. We therefore generated a humanized anti-human α9 Ab, termed ASP5094, and examined its pharmacological potential. ASP5094 inhibited the adhesion of SW480 cells stably expressing human α9 to Tn-C–derived peptide (Tn-Cfn3/RAA) in a concentration-dependent manner (IC_{50} of 3.87 ng/ml, Fig. 7A). Notably, ASP5094 suppressed the self-directed formation of multiple-layered assembly of RA-FLSs and converted these cells to single cell–layered lining such as OA-FLSs (Figs. 1A, 7B). ASP5094 resulted in a concentration-dependent reduction in the thickness of the lining-like structure of RA-FLSs in 3D culture (Fig. 7C, 7D). Neither etanercept, a TNF-α blocking agent, nor natalizumab, an integrin α4–blocking agent, exerted such effects at concentrations up to 10 and 100 μg/ml, respectively (Fig. 7C, 7D). These results indicate that the blockade of human α9 by ASP5094 can suppress development of a thickened synovial lining-like structure in 3D culture strongly suggest a possible pharmacological potential of ASP5094 in the treatment of RA-associated synovitis.

Discussion

RA is a severe debilitating autoimmune disease. Although there are several effective therapies for RA, these treatments all are limited by their immunosuppressive effects and the associated risks for infection and cancer. As such, there is a significant unmet medical need for effective RA therapies that are not by themselves immunosuppressive. RA-FLSs comprise the cellular lining of the joint, which becomes chronically inflamed and hyperplastic in RA. Therefore, treatments targeting RA-FLSs hyperplasia may represent a significant improvement in the treatment of RA without suppressing immune function.

The present study showed that RA-FLSs when maintained in 3D culture retained their disease-associated aggressive behavior, that is, self-directed formation of condensed lining architecture and autonomous production of proinflammatory mediators. In the 3D-culture system, RA-FLSs form thickened lining-like architecture that is not present in OA-FLSs grown under similar conditions (Fig. 1A, 1C). This thickened lining-like structure was comparable to that seen in synovial tissues from RA patients. In addition to these structural changes, the RA-FLSs grown in 3D culture showed an increased expression of *ITGA9* and *TNC* (Fig. 3A). Elevated expression and functional involvement of α9 and Tn-C in the development of ankle joint swelling was also confirmed in the CAIA model, where administration of mouse α9-blocking Ab suppressed synovial lining hyperplasia, bone resorption, and proinflammatory gene expression (Fig. 6A–D). It is therefore

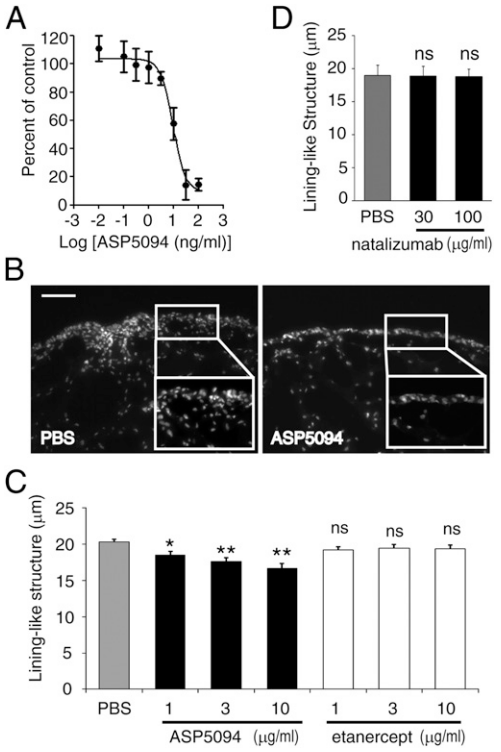

FIGURE 7. Pharmacological profile of ASP5094, a blocking Ab for α9. (**A**) Inhibition of adhesion of α9-expressing SW480 cells to plate coated with Tn-C peptide by ASP5094. A representative fitting curve from three independent experiments is shown. Each plot represents mean of quadruplicate assays with SD. (**B**–**D**) RA-FLSs were pretreated with ASP5094, etanercept, or natalizumab at indicated concentrations and 3D cultured in media containing the corresponding reagents. An equal volume of PBS was used as a control. (B) Typical images of the lining-like structure formed by RA-FLSs treated with PBS (left) or ASP5094 (10 μg/ml, right) stained with DAPI. Scale bar, 100 μm. (C and D) The thickness of the lining-like structure of the resultant architectures was calculated by image analyses and expressed as mean ± SE. (B), $n = 9$; (C), $n = 5$. Statistical analyses were performed by a Dunnett test using within-subject error. $*p < 0.05$, $**p < 0.01$. ns, not significant.

likely that RA-FLSs generate a Tn-C–rich ECM environment, to which RA-FLSs bind via α9 that they overexpressed. Interestingly, the expression of Tn-C was dependent on that of α9 in both 3D-cultured RA-FLSs (Fig. 4A) and CAIA joint (Fig. 6C). These results suggest that the engagement of α9 with Tn-C (Tn-C/α9 axis) triggers a self-amplifying positive feedback loop (Tn-C/α9 loop) and facilitates formation of the Tn-C–rich ECM environment, driving continuous expansion of pathogenic lining. The lining layer assembly of RA-FLSs requires not only cell–ECM adhesion but also cell–cell adhesion, and cadherin-11 is shown to be essential in the latter process (7). Intriguingly, we have found that depletion of either α9 or Tn-C resulted in decreased expression of cadherin-11 (Fig. 4B) and that administration of an α9-blocking Ab inhibited joint induction of *Chd11* in the CAIA model (Fig. 6E). The Tn-C/α9 axis is thus involved also in cadherin-11 expression and contributes to interaction between RA-FLSs for establishment of multilayered lining structure.

In addition to the essential role of the Tn-C/α9 axis in formation of structural assembly of RA-FLSs, we have found that the Tn-C/α9 axis is also crucial in their autonomous induction of proinflammatory gene expression. The 3D-cultured RA-FLSs showed not only phosphorylation of FAK but also upregulation of *MMP1*, *MMP3*, and *IL6* (Figs. 1D, 2B). The enhanced expression of these proinflammatory genes was suppressed by treatment with FAKi, indicating that FAK activation mediated induction of these genes (Fig. 2C). Notably, this proinflammatory behavior was abolished by depletion of α9 or Tn-C (Fig. 3C, 3D). Administration of an α9-blocking Ab in the CAIA model also inhibited phosphorylation of FAK as well as induction of *Mmp3* and *Il6* in the arthritic joints (Fig. 6D, 6E). Given the abundant expression of α9 and Tn-C in 3D-cultured RA-FLSs, these findings suggest that the Tn-C/α9 axis enhances activation of integrin signaling and upregulates proinflammatory gene expression in the synovial lining layer in RA.

Activation of α9 signaling in RA-FLSs also appears to sensitize these cells to external inflammatory stimuli. Evidence supporting this conclusion is based on the observation that shRNA that inhibited the synthesis of α9 abrogated PDGF-induced hyperplasia of RA-FLSs and blunted the TNF-α–mediated increase in proinflammatory mediator (MMP-1, MMP-3, and IL-6) production (Fig. 5). This suggests the involvement of α9-mediated integrin signaling in the cellular response to PDGF and TNF-α. One of the key players linking these pathways might be FAK. Previous reports described a critical role of FAK in cellular response of fibroblasts to PDGF and TNF-α. For example, pharmacological inhibition of FAK inhibits PDGF-induced proliferation of lung fibroblasts (38) and TNF-α–induced production of proinflammatory mediators in periodontal ligament fibroblasts (39). In this context, it is thought that α9-dependent autonomous activation of FAK in self-directed cell assembly potentiates the passive response of RA-FLSs to upstream stimuli, cytokines, and growth factors, leading to an amplified inflammatory response.

Collectively, our data thus clearly show that blockade of α9 is a promising approach to treat synovial inflammation in RA through suppression of the pathogenic behavior of RA-FLSs. ASP5094 may provide an innovative therapeutic approach for the unmet medical need of treatments for synovitis associated with RA.

Acknowledgments

We thank Toshihiro Nakashima, Hirofumi Higuchi, Masaharu Torikai, and Daisuke Ishikawa at the Chemo-Sero-Therapeutic Research Institute for protein generation and analysis of MA9-413 and for useful discussion on its use. We thank Ikuko Sasaki for establishment of the cell line stably expressing human α9. We appreciate the critical reading by Moritoshi Furu, Yoshitaka Hirayama, Yasutomo Fujii, Robert Townsend, and Marlowe Schneidkraut.

Disclosures

T.E., J.H., K.I., J.-i.Y., T.S., S.S., H.F., N.Y., Y.M., and I.A. are employees of Astellas Pharma Inc. S.N. is a scientific advisor to Astellas Pharma Inc. H.F. and N.Y. have patents for ASP5094 and MA9-413. H.I. has a grant from Bristol-Myers Squibb Co., Ltd. outside this work. M.H. has grants from Chugai Pharmaceutical Co., Ltd., Eisai Co. Ltd., and Abbvie GK outside this work. The other authors have no financial conflicts of interest.

References

1. Bartok, B., and G. S. Firestein. 2010. Fibroblast-like synoviocytes: key effector cells in rheumatoid arthritis. *Immunol Rev.* 233: 233–255.
2. Bellis, E., C. A. Scirè, G. Carrara, A. Adinolfi, A. Batticciotto, A. Bortoluzzi, G. Cagnotto, M. Caprioli, M. Canzoni, F. P. Cavatorta, et al. 2016. Ultrasound-detected tenosynovitis independently associates with patient-reported flare in patients with rheumatoid arthritis in clinical remission: results from the observational study STARTER of the Italian society for rheumatology. *Rheumatology* 55: 1826–1836.
3. Lisbona, M. P., A. Solano, J. Ares, M. Almirall, T. C. Salman-Monte, and J. Maymó. 2016. ACR/EULAR definitions of remission are associated with lower residual inflammatory activity compared with DAS28 remission on hand MRI in rheumatoid arthritis. *J. Rheumatol.* 43: 1631–1636.
4. Vreju, F. A., E. Filippucci, M. Gutierrez, L. Di Geso, A. Ciapetti, M. E. Ciurea, F. Salaffi, and W. Grassi. 2016. Subclinical ultrasound synovitis in a particular joint is associated with ultrasound evidence of bone erosions in that same joint in rheumatoid patients in clinical remission. *Clin. Exp. Rheumatol.* 34: 673–678.

5. Bottini, N., and G. S. Firestein. 2013. Duality of fibroblast-like synoviocytes in RA: passive responders and imprinted aggressors. *Nat. Rev. Rheumatol.* 9: 24–33.
6. Lefevre, S., F. M. Meier, E. Neumann, and U. Muller-Ladner. 2015. Role of synovial fibroblasts in rheumatoid arthritis. *Curr. Pharm. Des.* 21: 130–141.
7. Kiener, H. P., D. M. Lee, S. K. Agarwal, and M. B. Brenner. 2006. Cadherin-11 induces rheumatoid arthritis fibroblast-like synoviocytes to form lining layers in vitro. *Am. J. Pathol.* 168: 1486–1499.
8. Lee, D. M., H. P. Kiener, S. K. Agarwal, E. H. Noss, G. F. Watts, O. Chisaka, M. Takeichi, and M. B. Brenner. 2007. Cadherin-11 in synovial lining formation and pathology in arthritis. *Science.* 315: 1006–1010.
9. Chang, S. K., Z. Gu, and M. B. Brenner. 2010. Fibroblast-like synoviocytes in inflammatory arthritis pathology: the emerging role of cadherin-11. *Immunol. Rev.* 233: 256–266.
10. Qin, S., F. Wang, M. Zhou, W. Ding, L. Chen, and Y. Lu. 2015. Immunolocalization of membrane-type 1 MMP in human rheumatoid synovium tissues. *Int. J. Clin. Exp. Pathol.* 8: 9286–9292.
11. Takayanagi, H., H. Iizuka, T. Juji, T. Nakagawa, A. Yamamoto, T. Miyazaki, Y. Koshihara, H. Oda, K. Nakamura, and S. Tanaka. 2000. Involvement of receptor activator of nuclear factor κB ligand/osteoclast differentiation factor in osteoclastogenesis from synoviocytes in rheumatoid arthritis. *Arthritis Rheum.* 43: 259–269.
12. Lowin, T., and R. H. Straub. 2011. Integrins and their ligands in rheumatoid arthritis. *Arthritis Res Ther.* 13: 244.
13. Rinaldi, N., D. Weis, B. Brado, M. Schwarz-Eywill, M. Lukoschek, A. Pezzutto, U. Keilholz, and T. F. Barth. 1997. Differential expression and functional behaviour of the αv and β3 integrin subunits in cytokine stimulated fibroblast-like cells derived from synovial tissue of rheumatoid arthritis and osteoarthritis in vitro. *Ann. Rheum. Dis.* 56: 729–736.
14. Miranti, C. K., and J. S. Brugge. 2002. Sensing the environment: a historical perspective on integrin signal transduction. *Nat. Cell Biol.* 4: E83–E90.
15. Gupta, S. K., and N. E. Vlahakis. 2009. Integrin α9β1 mediates enhanced cell migration through nitric oxide synthase activity regulated by Src tyrosine kinase. *J. Cell. Sci.* 122: 2043–2054.
16. Velling, T., S. Nilsson, A. Stefansson, and S. Johansson. 2004. β1-Integrins induce phosphorylation of Akt on serine 473 independently of focal adhesion kinase and Src family kinases. *EMBO Rep.* 5: 901–905.
17. Yokosaki, Y., E. L. Palmer, A. L. Prieto, K. L. Crossin, M. A. Bourdon, R. Pytela, and D. Sheppard. 1994. The integrin α9β1 mediates cell attachment to a non-RGD site in the third fibronectin type III repeat of tenascin. *J. Biol. Chem.* 269: 26691–26696.
18. Smith, L. L., H. K. Cheung, L. E. Ling, J. Chen, D. Sheppard, R. Pytela, and C. M. Giachelli. 1996. Osteopontin N-terminal domain contains a cryptic adhesive sequence recognized by $\alpha_9\beta_1$ integrin. *J. Biol. Chem.* 271: 28485–28491.
19. Vlahakis, N. E., B. A. Young, A. Atakilit, and D. Sheppard. 2005. The lymphangiogenic vascular endothelial growth factors VEGF-C and -D are ligands for the integrin α9β1. *J. Biol. Chem.* 280: 4544–4552.
20. Staniszewska, I., S. Zaveri, L. Del Valle, I. Oliva, V. L. Rothman, S. E. Croul, D. D. Roberts, D. F. Mosher, G. P. Tuszynski, and C. Marcinkiewicz. 2007. Interaction of α9β1 integrin with thrombospondin-1 promotes angiogenesis. *Circ. Res.* 100: 1308–1316.
21. Asano, T., N. Iwasaki, S. Kon, M. Kanayama, J. Morimoto, A. Minami, and T. Uede. 2014. α9β1 Integrin acts as a critical intrinsic regulator of human rheumatoid arthritis. *Rheumatol.* 53: 415–424.
22. Kanayama, M., D. Kurotaki, J. Morimoto, T. Asano, Y. Matsui, Y. Nakayama, Y. Saito, K. Ito, C. Kimura, N. Iwasaki, et al. 2009. α9 Integrin and its ligands constitute critical joint microenvironments for development of autoimmune arthritis. *J. Immunol.* 182: 8015–8025.
23. Perlman, H., and R. M. Pope. 2010. The synovial lining micromass system: toward rheumatoid arthritis in a dish? *Arthritis Rheum.* 62: 643–646.
24. Alsalameh, S., R. J. Amin, E. Kunisch, H. E. Jasin, and R. W. Kinne. 2003. Preferential induction of prodestructive matrix metalloproteinase-1 and proinflammatory interleukin 6 and prostaglandin E_2 in rheumatoid arthritis synovial fibroblasts via tumor necrosis factor receptor-55. *J. Rheumatol.* 30: 1680–1690.
25. Kiener, H. P., G. F. Watts, Y. Cui, J. Wright, T. S. Thornhill, M. Skold, S. M. Behar, B. Niederreiter, J. Lu, M. Cernadas, et al. 2010. Synovial fibroblasts self-direct multicellular lining architecture and synthetic function in three-dimensional organ culture. *Arthritis Rheum.* 62: 742–752.
26. Uehara, K., H. Higuchi, T. Nakashima, D. Ishikawa, N. Yamamoto, H. Fujita, and F. Sakai. 2009. Improved humanized anti-human α9-integrin antibody. United States patent application PCT/JP2009/050187, Publication No. WO2009088064A1. 2009 July 16.
27. Altman, R., E. Asch, D. Bloch, G. Bole, D. Borenstein, K. Brandt, W. Christy, T. D. Cooke, R. Greenwald, M. Hochberg, et al; Diagnostic and Therapeutic Criteria Committee of the American Rheumatism Association. 1986. Development of criteria for the classification and reporting of osteoarthritis. Classification of osteoarthritis of the knee. *Arthritis Rheum.* 29: 1039–1049.
28. Arnett, F. C., S. M. Edworthy, D. A. Bloch, D. J. McShane, J. F. Fries, N. S. Cooper, L. A. Healey, S. R. Kaplan, M. H. Liang, H. S. Luthra, et al. 1988. The American rheumatism association 1987 revised criteria for the classification of rheumatoid arthritis. *Arthritis Rheum.* 31: 315–324.
29. Shibuya, H., H. Yoshitomi, K. Murata, S. Kobayashi, M. Furu, M. Ishikawa, T. Fujii, H. Ito, and S. Matsuda. 2015. TNFα, PDGF, and TGFβ synergistically induce synovial lining hyperplasia via inducible PI3Kδ. *Mod. Rheumatol.* 25: 72–78.
30. Montero-Melendez, T., and M. Perretti. 2014. Gapdh gene expression is modulated by inflammatory arthritis and is not suitable for qPCR normalization. *Inflammation.* 37: 1059–1069.
31. Choe, J. Y., B. Crain, S. R. Wu, and M. Corr. 2003. Interleukin 1 receptor dependence of serum transferred arthritis can be circumvented by Toll-like receptor 4 signaling. *J. Exp. Med.* 197: 537–542.
32. Banda, N. K., B. Levitt, M. J. Glogowska, J. M. Thurman, K. Takahashi, G. L. Stahl, S. Tomlinson, W. P. Arend, and V. M. Holers. 2009. Targeted inhibition of the complement alternative pathway with complement receptor 2 and factor H attenuates collagen antibody-induced arthritis in mice. *J. Immunol.* 183: 5928–5937.
33. McMorrow, J. P., D. Crean, M. Gogarty, A. Smyth, M. Connolly, E. Cummins, D. Veale, U. Fearon, P. P. Tak, O. Fitzgerald, and E. P. Murphy. 2013. Tumor necrosis factor inhibition modulates thrombospondin-1 expression in human inflammatory joint disease through altered NR4A2 activity. *Am. J. Pathol.* 183: 1243–1257.
34. Cha, H. S., E. K. Bae, J. H. Koh, J. Y. Chai, C. H. Jeon, K. S. Ahn, J. Kim, and E. M. Koh. 2007. Tumor necrosis factor-alpha induces vascular endothelial growth factor-C expression in rheumatoid synoviocytes. *J. Rheumatol.* 34: 16–19.
35. Wu, M., T. Xu, Y. Zhou, H. Lu, and Z. Gu. 2013. Pressure and inflammatory stimulation induced increase of cadherin-11 is mediated by PI3K/Akt pathway in synovial fibroblasts from temporomandibular joint. *Osteoarthritis Cartilage.* 21: 1605–1612.
36. Torikai, M., D. Ishikawa, T. Nakashima, H. Higuchi, F. Sakai, N. Yamamoto, H. Fujita, and K. Taguchi. 2009. Human anti-α9 integrin antibody. United States patent application PCT/JP2008/073825, Publication No. WO2009084671A1. 2009 July 9.
37. Khachigian, L. M. 2006. Collagen antibody-induced arthritis. *Nat. Protoc.* 1: 2512–2516.
38. Kinoshita, K., Y. Aono, M. Azuma, J. Kishi, A. Takezaki, M. Kishi, H. Makino, H. Okazaki, H. Uehara, K. Izumi, et al. 2013. Antifibrotic effects of focal adhesion kinase inhibitor in bleomycin-induced pulmonary fibrosis in mice. *Am. J. Respir. Cell Mol. Biol.* 49: 536–543.
39. Zhang, P., Y. J. Li, L. Y. Guo, G. F. Wang, K. Lu, and E. L. Yue. 2015. Focal adhesion kinase activation is required for TNF-α-induced production of matrix metalloproteinase-2 and proinflammatory cytokines in cultured human periodontal ligament fibroblasts. *Eur. J. Oral Sci.* 123: 249–253.